7.4 A STUDY ON THE IMPACT OF TROPOSPHERIC CLOUD SYSTEMS ON ANTARCTIC POLAR STRATOSPHERIC CLOUDS USING NASA A-TRAIN CLOUDSAT AND CALIPSO MEASUREMENTS

Loknath Adhikari* and Zhien Wang
University of Wyoming, Laramie, WY

1. INTRODUCTION

Polar stratospheric clouds (PSC) started attracting considerable attention from the scientific community after the discovery of ozone hole in 1985 and the subsequent evidences that showed significant roles of PSCs in the depletion of stratospheric ozone. Studies done so far on PSCs have provided valuable information based on laboratory investigations e.g. Hanson & Mauersberger (1988), Tabazadeh et al. (2000), in-situ measurements (Larsen et al., 2000), modeling (Svendsen et al., 2005) and remote sensing (Fromm et al., 1997, 1999, 2003; Teitelbaum et al., 2001; Spang et al., 2005). Recent advancement in satellite remote sensing using lidars and radar has greatly increased our potential to better understand PSCs because they overcome the shortcomings of passive remote sensing including limb measurements and surface-based lidar measurements. Satellite based lidars have better horizontal resolution than limb measurements and better spatial coverage than surface-based lidar measurements. NASA A-train constellation that include Cloud-Aerosol Lidar and Infrared Pathfinder Satellite Observations (CALIPSO) (Winker et al., 2003) and CloudSat (Stephens et al., 2002) satellites provide an unprecedented ability to study PSCs and tropospheric clouds in the Polar Regions. CALIPSO and CloudSat carry depolarization-capable dual wavelength lidar, Cloud-Aerosol Lidar with Orthogonal Polarization (CALIOP) and a 94-GHz Cloud Profiling Radar (CPR), respectively. Different sensitivities of lidar and radar to drop size distribution and number concentration provide data suitable for understanding association of tropospheric clouds and PSCs.

The association of tropospheric clouds on PSCs has been recognized in previous scientific investigations, e.g. Teitelbaum et al. (2001), Wang et al. (2008) and many other authors. Teitelbaum et al. (2001) used Polar Ozone and Aerosol Measurement (POAM II) and Television Infrared Observation Satellites (TIROS) Operational Vertical Sounders (TOVS) data in the Arctic region and showed that the presence of potential vorticity anomalies near the tropopause cause quasi-adiabatic uplift through the lower stratosphere causing adiabatic cooling in the stratosphere. The local cooling events can provide suitable conditions for PSC formation; however, the extent to which tropospheric meteorology or tropospheric cloudiness affects PSCs is not well realized or understood.

*corresponding author address: Loknath Adhikari, 1000 E University Ave., Dept 3038, Laramie, WY 82072; email: loknath@uwyo.edu

In the present study, the evolution of PSCs is investigated. PSCs are classified in to different CALIPSO-based classes and the effects of tropospheric cloud systems on the distribution and the microphysical properties of these PSC classes are investigated.

2. DATA ANALYSIS

CALIPSO and CloudSat measurements taken during the periods from June through September of 2006 and 2007 are used in the study. Temperature measurements from the same period are taken from the microwave limb sounder abroad Aura satellite, another satellite in the NASA A-train constellation.

CALIPSO level 1B and CloudSat 2B-GEOPROF data are used in the analysis. CALIPSO level 1B data have height dependent vertical and horizontal resolution, so for consistency the vertical resolution of CALIPSO profiles have been averaged to 180 m for all the levels from -0.5 to 30.1 km. Then the CALIPSO profiles are collocated to CloudSat footprint (1.4 km across × 1.8 km along track) and averaged to form a collocated CloudSat-CALIPSO database. CloudSat radar bins with cloud mask values ≥ 30 are used to identify cloudy bins from radar. Attenuated lidar scattering ratio (ALSR), which is the ratio of the total attenuated backscattering coefficient to the molecular-only attenuated backscattering coefficient, is used for generating cloud mask from lidar measurements. Simple threshold method is applied in the detection of clouds from lidar as described in Wang et al. (2008).

Detection of PSCs is performed by using a simple threshold on the calculated ALSR values. CALIPSO data is moving averaged to a horizontal resolution of 20 km to improve the signal-to-noise ratio for ALSR. For night-time measurements a threshold of 1.8 is taken and for day-time measurements a threshold of 4 is set to exclude the effect of solar noise.

The optical and microphysical properties are analyzed based on the estimated PSC depolarization ratio, backscattering coefficient and the color ratio (ratio of backscattering coefficients of 1064 and 532 nm channels). The PSC depolarization ratio (δ') is estimated by eliminating the effect of molecular scattering on the volume depolarization ratio (δ), given by

$$\delta' = \frac{R\delta - \delta_m}{R + \delta_m - \delta - 1}$$

where, R and δ_m (0.0035) are ALSR and depolarization ratio signal for the molecular signal respectively.

The PSC backscattering coefficient is estimated from total attenuated backscattering coefficient provided in the CALIPSO level 1B data by correcting for attenuation and then subtracting the molecular backscattering. The attenuation correction is done by estimating the extinction coefficient by using a lidar ratio (ratio of extinction to backscatter) of 25. The lidar ratio is a function of particle size and particle type, so using a constant lidar ratio may result in large uncertainties in some cases. However, the impact on the estimated PSC backscattering is small because of the small optical depth of the PSCs and the attenuation corrections are typically within 20 %.

PSC classification is based on the classification scheme described by Pitts et al. (2009), which uses PSC backscattering coefficient and inverse of the ALSR. Based on this classification, PSCs are classed in to four classes, viz. STS, Mix 1, Mix 2 and ice. Figure 1 shows the thresholds used to distinguish the four classes of PSCs.

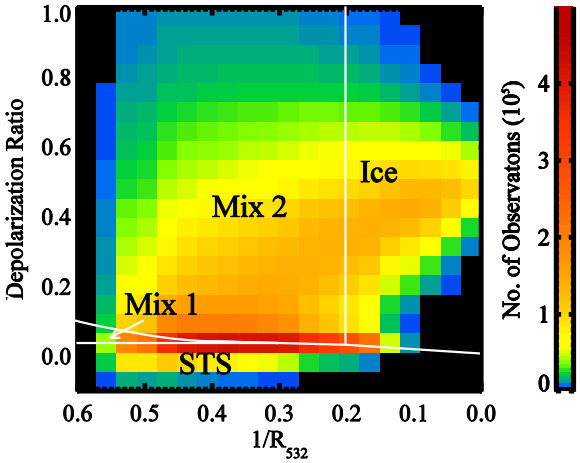

Figure 1: Classification of PSC into based on 1/ALSR and depolarization ratio values

3. RESULTS AND DISCUSSION

PSCs start to appear by late May and persist until late September/early October. They are ubiquitous in the region; however, there are localized areas that show high occurrences. Figure 2 shows monthly distribution of PSC occurrences for June through September of 2006 and 2007. The figure reveals that there is a high spatial variability of PSC occurrences among different months and between the two years. These localized areas of high PSC occurrence indicate the possible role of mesoscale dynamical events in controlling the distribution of PSCs. Comparison with the mean cyclonic behavior in the southern hemisphere compiled by Simmonds and Keay (2000) reveal that these localized areas of high PSC occurrences lie in the regions downwind of the regions that show high cyclonic activities.

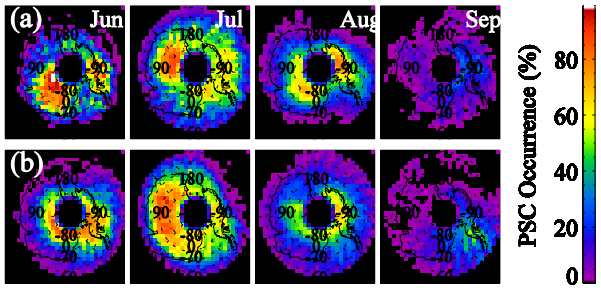

Figure 2: Monthly PSC occurrence (%) for (a) 2006 and (b) 2007.

The evolution of PSCs in the Antarctic stratosphere closely follows the lower stratospheric temperature evolution. The stratosphere begins to cool gradually from early may and by late May/early June the temperature around 20 km level cools to below 200 K, with temperatures at that level as low as 190 K in the interior continental region. Figure 3 shows a time-height distribution of PSC occurrence 2007 and the mean and minimum temperatures for the whole region south of 60°S at 46 hPa (~ 20 km) levels. PSCs start to appear around 20 – 25 km level by late May at 20 – 25 km altitude range. By July, PSCs appear at elevations as low as 12 km, but highest occurrences are in the 18 – 24 km range. In the later part of the season, late August and September PSCs are confined to lower stratosphere, in the altitude range 12 – 16 km. The time series of PSC occurrence shows a highly cellular structure that cannot be explained by the temperature evolution alone. Topographically forced mountain waves have been linked to PSC formation (Cariolle et al., 1989, Carslaw et al., 1998). However, these PSCs formed by mountain waves tend to remain quasi-stationary and do not sufficiently explain the high monthly and inter-annual variability in PSC occurrence shown in Fig. 2. Tropospheric cloudiness can be a possible reason for PSC occurrence and distribution as illustrated in Fig. 3 (a). The high PSC occurrences are closely associated with tropospheric cloudiness as shown by the cross-sectional area along satellite tracks for tropospheric high level and deep clouds. Further statistical analysis between PSC area and tropospheric cloud area, both expressed as cross-sectional area along satellite tracks, show that the linear correlation coefficients for 2007 is 79 %. The linear correlation coefficient between tropospheric cloud area and PSC area for 2006 (not shown in figure) is 78 %. The high correlation coefficients for both the years also indicate that tropospheric cloudiness affect PSC formation and distribution in the Antarctic region.

Areal coverage of PSCs increases from the start of PSC onset in late May until late July or early August and decreases sharply by middle of August, when the stratospheric temperature starts to rise. The role of quasi-adiabatic cooling associated with tropospheric cloudiness becomes more important for PSCs after this rise in stratospheric temperatures. PSCs associated with tropospheric cloud systems account for about 50 % of the total PSCs for most of the PSC season, however,

by early September 60 – 70 % of all PSCs are associated with tropospheric cloud systems.

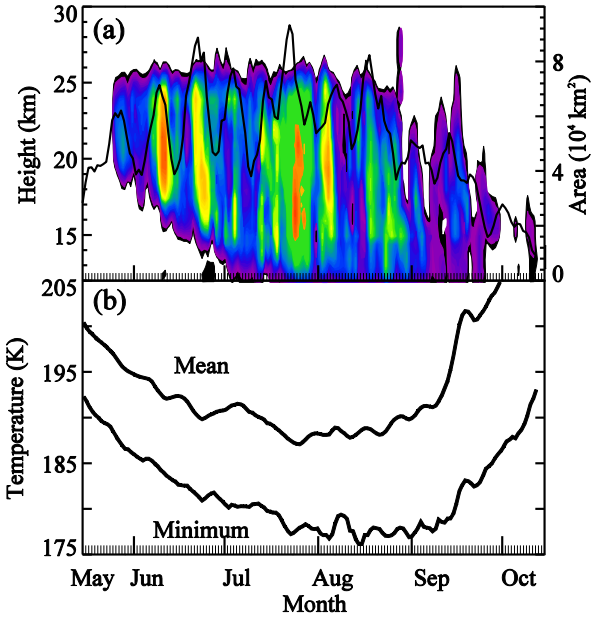

Figure 3: (a) Daily average vertical distribution of PSC occurrence for 2007. The solid black line shows daily tropospheric high-level and deep cloud area under satellite track. (b) Daily variation of mean and minimum temperatures at 46 hPa (~ 20 km) level for the region south of 60 °S.

The distribution of different PSC classes and their microphysical properties are affected by tropospheric cloudiness as illustrated in Figures 4 and 5. Figure 4 shows monthly count of the four PSC classes for PSCs associated and not associated with tropospheric cloud systems for June through October of 2006. In the early PSC season (June through August), STS, Mix 1 and Mix 2 similar number of observations for PSCs associated and not associated with tropospheric clouds. However, the number of ice PSCs is larger for PSCs associated with tropospheric clouds than for PSCs not associated with tropospheric clouds during all the months from June through October. Ice PSCs, which are dominated by ice particles, require much colder temperatures to form than the other three PSC classes. Hence, the additional cooling the tropospheric cloud systems can provide becomes important for ice PSCs. During September and October, when stratospheric temperatures are warmer more than 80 % of all the PSC classes are associated with tropospheric clouds.

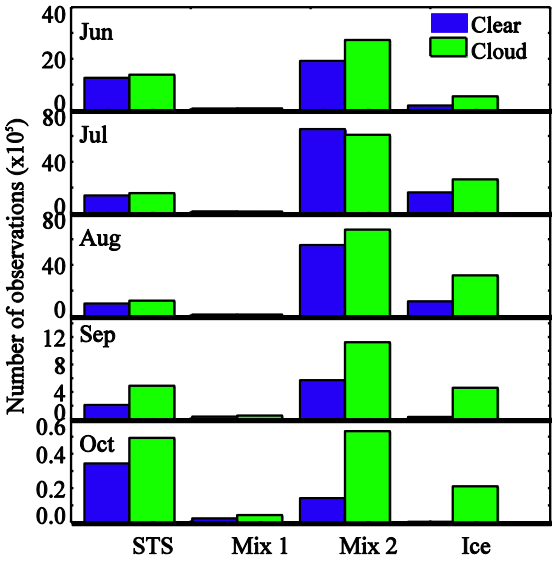

Figure 4: Histograms showing monthly distribution of Observed occurrence of different classes of PSCs for 2006.

Figure 5 shows probability density functions (PDF) of backscattering coefficient and color ratio for the four PSC classes for the months of June through October of 2006. T-test was applied to test the statistical significance of whether the backscattering coefficient and color ratio have similar means for clouds associated and not associated with tropospheric clouds. Both the backscattering coefficient and the color ratio are significantly different at 0.05 significant level for ice PSCs in all the months except in July. There is no significant difference at 0.05 significant level in the means of both backscattering coefficients and color ratio of STS and Mix 1 classes associated and not associated with tropospheric clouds. In the case of Mix 2, significant differences in the mean (at 0.05 significant level) exist for backscattering coefficient, but not for color ratio for later months.

The figure shows that the backscattering coefficients for PSCs associated with clouds are larger than for PSCs not associated with clouds. However, the color ratios have similar values for PSCs associated and not associated with tropospheric clouds. A smaller impact on the color ratio for all the PSC classes associated and not associated with tropospheric clouds indicates similar effective particle size. In all four PSC classes, especially for Mix 2 and ice, PSCs associated with tropospheric clouds have larger backscattering coefficients than PSCs not associated with tropospheric clouds. A small change in color ratio accompanied by an increase in the backscattering coefficient indicates an increased PSC number concentration. Hence, PSCs associated with tropospheric clouds are more likely to have a higher number concentration than PSCs not associated with tropospheric clouds. A higher particle concentration provides a larger surface area for stratospheric heterogeneous chemical reactions, leading to more ozone loss processes (Carslaw et al., 1998).

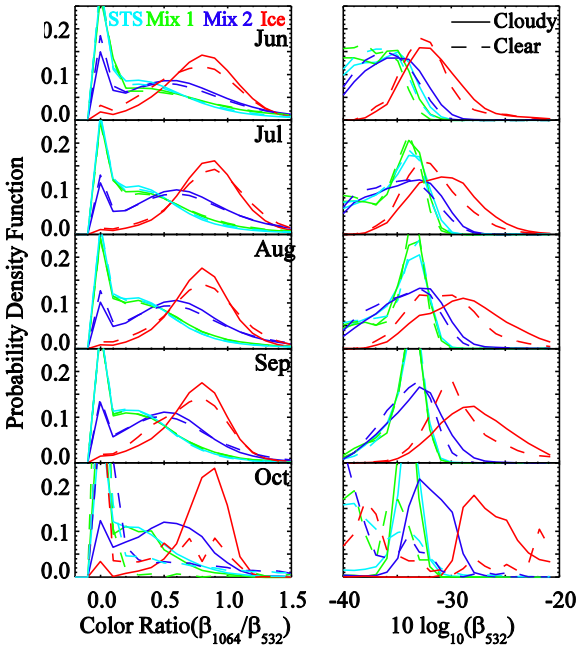

Figure 5: Probability density function of color ratio (β_{1064}/β_{532}) and 10 $\log_{10}\beta_{532}$ (backscattering coefficients, km^{-1} Sr^{-1})

4. SUMMARY

PSCs in the Antarctic region form in the polar winter night and remain until early October. Although cooling within the polar vortex is the main mechanism for the formation of PSCs, new NASA satellite data indicate that PSC occurrence and chemical and microphysical properties are also strongly associated with deep tropospheric cloud systems.

ALSR values calculated from CALIPSO lidar measurements were used to identify PSCs, while combined CloudSat and CALIPSO data were used to identify tropospheric cloud systems. PSCs were classified into four classes, viz. STS, Mix 1, Mix 2 and ice, based on volume depolarization ratio and inverse ALSR values.

PSCs start to appear by the end of May in the lower stratosphere at 18 – 25 km with predominantly STS particles and gradually extend to lower altitudes with more frequent NAT/STS mixtures and ice particles. By early September PSCs are mostly confined to elevation below 20 km and they completely dissipate by early/mid October. The highest PSC occurrence (in terms of PSC area under satellite track) is observed during late July to early August.

PSCs are ubiquitous in the Antarctic stratosphere during austral winter; however, there are localized areas of high PSC occurrence. These high PSC occurrence areas show monthly and inter-annual variabilities. The presence of localized high PSC occurrence areas indicates the roles of mesoscale dynamics in PSC formation. These high PSC occurrence areas lie in the regions downwind of heavy cyclonic activities in the Antarctic coast. Deep tropospheric clouds provide additional cooling in the low stratosphere, favoring PSC formation (Teitelbaum et al., 2001; Wang et al., 2008). The high correlation coefficient of 0.78 and 0.79 between PSC area and tropospheric cloudiness for 2006 and 2007 PSC seasons in the Antarctic region is indicative of the roles tropospheric clouds play in PSC formation.

Cooling associated with tropospheric clouds also affects the relative occurrence of different PSC classes and their microphysical properties, especially during September and October, when the lower stratospheric temperatures start to warm up. During September and October 60 – 70 % of all PSC classes are associated with tropospheric clouds, whereas during the first three months (June through August) ~ 50 % of PSCs are associated with tropospheric clouds. PSC class ice, which requires colder temperatures to form, is most affected by tropospheric clouds. All five months have higher occurrence of PSC class ice associated with tropospheric clouds. During September and October, ~ 80 % of PSC class ice is associated with tropospheric clouds. On the microphysical properties, the backscattering coefficient for PSCs associated with tropospheric clouds is larger than for PSCs not associated with tropospheric clouds, whereas there are not any significant differences in the color ratio between PSCs associated and not associated with tropospheric clouds.

5. REFERENCES

Cariolle, D., S. Muller, and F. Cayla (1989), Mountain waves, polar stratospheric clouds, and the ozone depletion over Antarctica, *J. Geophys. Res., 94*(D9), 11233-11240.

Carslaw, K. S., M. Wirth, A. Tsias, B. P. Luo, A. Dornbrack, M. Leutbecher, H. Volkert, W. Renger, J. T. Bacmeister, E. Reimer, T. Peter (1998), Increased stratospheric ozone depletion due to mountain-induced atmospheric waves, *Nature, 391,* 675-678.

Fromm, M. D., J. D. Lumpe, R. M. Bevilacqua, E. P. Shettle, J. Hornstein, S. T. Massie, K. H. Fricke (1997), Observations of Antarctic polar stratospheric clouds by POAM II: 1994-1996, *J. Geophys. Res., 102,* D19, 23659-23672.

Fromm, M. D., R. M. Bevilacqua, J. Hornstein, E. Shettle, K. Hoppel, J. D. Lumpe, (1999), An analysis of Polar Ozone and Aerosol Measurement (POAM) II arctic polar stratospheric cloud observation, 1993-1996, *J. Geophys. Res., 104,* D20, 24341-24357.

Fromm, M., J. Alfred, and M. Pitts (2003), A unified, long-term, high-latitude stratospheric aerosol and cloud database using SAM II, SAGE II, and POAM II/III data: Algorithm

Hanson, D. and K. Mauersberger (1988), laboratory studies of the nitric acid trihydrate: implications for the south polar stratosphere, *Geophys. Res. Letts., 15,* 855-858.

Larsen, N., I. S. Mikkelsen, B. M. Knudsen, J. Schreiner, C. Voigt, K. Mauersberger, J. M. Rosen, N. T. Kjome (2000), Comparison of chemical and optical in situ measurements of polar stratospheric cloud particles, *J. Geophys. Res., 105*(D1), 1491-1502.

Pitts, M. C., L. R. Poole, L. W. Thomason (2009), CALIPSO polar stratospheric cloud observations: Second generation detection algorithm and composition discrimination, *Atmos. Chem. Phys. Discuss., 9,* 8121-8157.

Simmonds, I. and Keay, K., 2000: Mean Southern Hemisphere extratropical cyclone behavior in the 40-year NCEP-NCAR reanalysis, *J. Climate,* **13,** 873-885.

Spang, R., J. J. Remedios, L. J. Kramer, L. R. Poole, M. D. Fromm, G. Baumgarten, P. Konopka (2005), Polar stratospheric clouds observations by MIPAS on ENVISAT: Detection method, validation and analysis of the northern hemisphere winter 2002/2003, *Atmos. Chem. Phys., 5,* 679-692.

Stephens, G. L., Vane, D. G. , Boain, R. J., Mace, G. G., Sassen, K. , Wang, Z., Illingworth, A. J., O'Conner, E. J., Rossow, W. G., Durden, S. L., Miller, S. D., Austin, R. T., Benedetti, A., Mitrescu, C., 2002: The CloudSat mission and the A-Train, *Bull. Amer. Meteorol. Soc.,* **83,** 1771–1790.

Svendsen, S. H., N. Larsen, B. Knudsen, S. D. Eckermann, E. V. Browell (2005), Influence of mountain waves and NAT nucleation mechanism on polar stratospheric cloud formation at local scales during the 1999-2000 Arctic winter, *Atmos. Chem. Phys., 5,* 739-753.

Tabazadeh, A., S. T. Martin, J-S Lin (2000), The effect of particle size and nitric acid uptake on the homogeneous freezing of aqueous sulfuric acid particles, *Geophys. Res. Letts., 27,* 1111-1114.

Teitelbaum, H., M. Moustaoui, M. Fromm (2001), Exploring polar stratospheric cloud and ozone minihole formation: The primary importance of synoptic-scale flow perturbation, *J. Geophys. Res., 106,* 28173-28188.

Wang, Z., Stephens, G., Deshler, T., Trepte, C., Parish, T., Vane, D., Winker, D., Liu, D., Adhikari, L., 2008: Association of Antarctic polar stratospheric cloud formation on tropospheric cloud systems, *Geophys. Res. Letts.,* **35,** L13806, doi:10.1029/2008GL034209.

Winker, D. M., Pelon, J. R., and McCormick, M. P., 2003: The CALIPSO mission: Spaceborne lidar for observation of aerosols and clouds, *Proc. SPIE,* 4893, 1–11.